Volume 14
Number 48
28 December 2023
Pages 13991–14328

Chemical Science

rsc.li/chemical-science

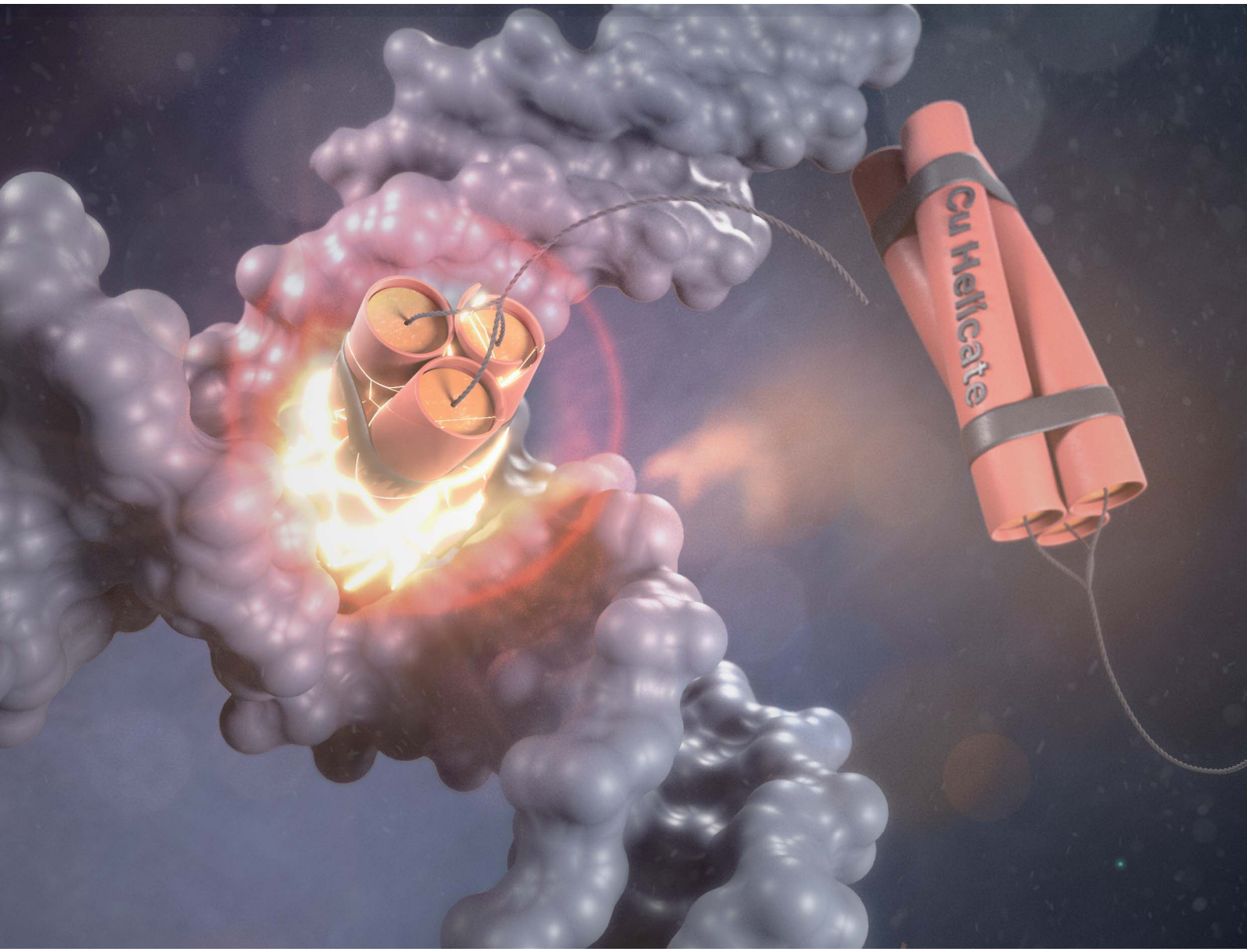

ISSN 2041-6539

ROYAL SOCIETY OF CHEMISTRY

EDGE ARTICLE

Andrew Kellett, José Martínez-Costas, Miguel Vázquez López *et al.*
A copper(II) peptide helicate selectively cleaves DNA replication foci in mammalian cells

Chemical Science

ROYAL SOCIETY OF CHEMISTRY

EDGE ARTICLE

View Article Online
View Journal | View Issue

Cite this: *Chem. Sci.*, 2023, **14**, 14082

All publication charges for this article have been paid for by the Royal Society of Chemistry

Received 29th June 2023
Accepted 25th October 2023

DOI: 10.1039/d3sc03303a

rsc.li/chemical-science

A copper(II) peptide helicate selectively cleaves DNA replication foci in mammalian cells†

Ana Alcalde-Ordóñez,‡[a] Natalia Barreiro-Piñeiro,‡[b] Bríonna McGorman,‡[c] Jacobo Gómez-González,‡[a] David Bouzada,[a] Francisco Rivadulla,[d] M. Eugenio Vázquez,[a] Andrew Kellett,*[c] José Martínez-Costas*[b] and Miguel Vázquez López*[e]

The use of copper-based artificial nucleases as potential anticancer agents has been hampered by their poor selectivity in the oxidative DNA cleavage process. An alternative strategy to solve this problem is to design systems capable of selectively damaging noncanonical DNA structures that play crucial roles in the cell cycle. We designed an oligocationic Cu^{II} peptide helicate that selectively binds and cleaves DNA three-way junctions (3WJs) and induces oxidative DNA damage *via* a ROS-mediated pathway both *in vitro* and *in cellulo*, specifically at DNA replication foci of the cell nucleus, where this DNA structure is transiently generated. To our knowledge, this is the first example of a targeted chemical nuclease that can discriminate with high selectivity 3WJs from other forms of DNA both *in vitro* and in mammalian cells. Since the DNA replication process is deregulated in cancer cells, this approach may pave the way for the development of a new class of anticancer agents based on copper-based artificial nucleases.

Introduction

The discovery of the cytotoxic properties of cisplatin by Barnett Rosenberg in 1965[1] gave rise to the new field of canonical dsDNA-targeted metallodrugs for cancer therapy.[2] More recently, as our knowledge of the structural polymorphism and biology of DNA expanded, the bioinorganic field has shifted towards targeting noncanonical DNA structures, including single-stranded DNA, i-motifs, G-quadruplexes (G4s), DNA triplexes and DNA junctions, such as three-way (3WJs) and four-way (Holliday) junctions, among others.[3–13] Here, we present a Cu^{II} peptide helicate that selective recognises 3WJs both *in vitro* and at DNA replication foci in mammalian cells. This is the first time such specificity has been achieved.

3WJs are the simplest branched DNA structures,[14] consisting of symmetrical assemblies formed by three convergent dsDNA units that meet at a central point called the branch point, which forms a hydrophobic cavity approximately 12 Å in diameter that is defined by the terminal base pairs of each of the three B-DNA arms.[15] Metallosupramolecular helicates are the most promising agents for the selective recognition of these noncanonical DNA structures.[6–12] One of the key factors for their selectivity is the high complementarity between their shape and the trigonal symmetry of the branch point of the 3WJs. Indeed, this is a key structural feature of other 3WJ binders, such as triptycene derivatives,[16] C_3-symmetric cationic azacryptands,[17] self-assembled supramolecular Fe^{II} tetrahedral metallocages[18] and three-fold symmetric tripeptides.[19]

3WJs participate in a number of key biological processes,[20–22] and notably they are transiently formed in the replication fork during DNA replication.[23] Therefore, 3WJ-binding ligands are expected to stall the replication fork and elicit genotoxic replication stress in rapidly dividing cells, such as tumoral ones.[24,25] For these reasons, 3WJs are currently considered a promising target for the development of new anticancer drugs with unique therapeutic properties.[26–31]

On the other hand, artificial Cu^{II} metallonucleases have been investigated as nucleic acid targeting drug molecules,[32,33] and there are several examples in the literature of Cu^{II} complexes[34–36] with remarkable anticancer activity combined with lower off-target toxicity than classical platinum drugs.[37] Copper

[a]*Centro Singular de Investigación en Química Biolóxica e Materiais Moleculares (CiQUS), Departamento de Química Orgánica, Universidade de Santiago de Compostela, 15782 Santiago de Compostela, Spain*

[b]*Centro Singular de Investigación en Química Biolóxica e Materiais Moleculares (CiQUS), Departamento de Bioquímica e Bioloxía Molecular, Universidade de Santiago de Compostela, 15782 Santiago de Compostela, Spain*

[c]*SSPC, The SFI Research Centre for Pharmaceuticals, School of Chemical Sciences, Dublin City University, Glasnevin, Dublin 9, Ireland*

[d]*Centro Singular de Investigación en Química Biolóxica e Materiais Moleculares (CiQUS), Departamento de Química Física, Universidade de Santiago de Compostela, 15782 Santiago de Compostela, Spain*

[e]*Centro Singular de Investigación en Química Biolóxica e Materiais Moleculares (CiQUS), Departamento de Química Inorgánica, Universidade de Santiago de Compostela, 15782 Santiago de Compostela, Spain. E-mail: miguel.vazquez.lopez@usc.es*

† Electronic supplementary information (ESI) available. See DOI: https://doi.org/10.1039/d3sc03303a

‡ These authors contributed equally.

nucleases produce reactive oxygen species (ROS) that can cleave dsDNA through two alternative mechanisms: hydrolysis of the phosphodiester backbone, or oxidative H-atom abstraction from the deoxyribose ring.[38] Copper-based nucleases themselves have little or no sequence selectivity,[39] which limits their therapeutic potential. Consequently extensive research has been performed to generate hybrid chemical nucleases that can target specific nucleic acid structures and sequences. This has previously involved the attachment of well-studied chemical nucleases to nucleic acid recognition moieties such as dsDNA groove binders,[40–43] non canonical DNA binders (specifically triplex DNA[44] and G-quadruplexes[45]) or sequence specific dsDNA targeting agents.[46–49] However, to date, no chemical nuclease, copper-derived or not, specifically directed against 3WJs has been described.

In 2021, we reported the first example of a chemical compound that selectively recognizes 3WJs in cells.[50] The oligocationic ligand precursor of the metal complex that exhibited such activity was equipped with six artificial 2,2′-bipyridine-derived metal-binding residues that can fold predictably in the presence of Fe^{II} ions giving rise to a stable, water soluble, chiral dinuclear peptide helicate. That Fe^{II} peptide helicate, **ΛΛ-Fe^{II}$_2$LLD** (Scheme 1), showed high affinity and selectivity towards 3WJs compared with canonical DNA *in vitro* and, importantly, selectively labelled DNA replication foci in the cell nuclei.[50] Inspired by this precedent, herein we describe a redox active Cu^{II} peptide helicate that exhibit highly precise nuclease activity towards 3WJs *in vitro*, and can selectively cleaves DNA replication foci in mammalian cells. To our knowledge, the system reported herein is the first example of a chemical nuclease that exhibits high cleavage selectivity for 3WJs from other forms of DNA both *in vitro* and in mammalian cells. Since cancer cells have a deregulated DNA replication process, this approach may lead to the development of a new class of anti-cancer agents based on copper-based artificial nucleases.

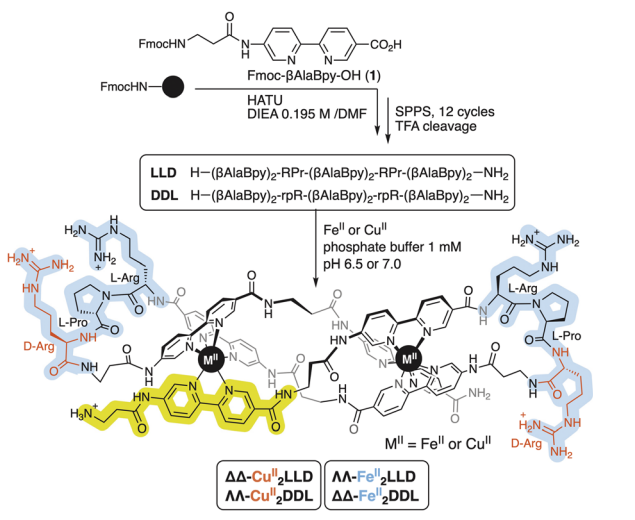

Scheme 1 Sequences of the peptide ligands **LLD** and **DDL** equipped with six units of the Fmoc-βAlaBpy-OH (**1**) coordinating residue. After their synthesis by SPPS methods, cleavage, and purification, the Cu^{II} helicates are stereoselectively folded under thermodynamic control in the presence of Cu^{II} ions. L-amino acids are indicated in upper-case, and D-amino acids in lower case (*i.e.*, R, P for L-Arg and L-Pro, and r for D-Arg). Heterochiral β-turn loops are highlighted in blue and one of the six coordinating residues (**1**) in yellow.

Results and discussion

Synthesis and characterization of the Cu^{II} peptide helicate

The precursor peptide ligand **LLD** was assembled using standard Fmoc solid-phase peptide synthesis procedures.[50] The Bpy ligand was introduced as an Fmoc-protected building block, Fmoc-βAlaBpy-OH (1; Scheme 1). The final peptide ligand was purified by HPLC, and its identity was confirmed by mass spectrometry (Fig. S1 and S5†).

The formation in solution of the **Cu^{II}$_2$LLD** peptide helicate (Scheme 1) was characterized by IR and UV spectroscopies (Fig. S3†) and by monitoring the quenching in the fluorescence emission band of the Bpy fluorophores present in **LLD** upon metal coordination (Fig. 1a and S4†). The resulting titration profile was fitted to a 1 : 2 (**LLD** : Cu^{II}) model with a global dissociation constant of approximately 34.3 (9.4) nM. MALDI spectra of the solution at saturating concentrations of Cu^{II} ions showed a peak at $m/z = 2555.97$, consistent with the formation of the **Cu^{II}$_2$LLD** peptide helicate (Fig. S4†).

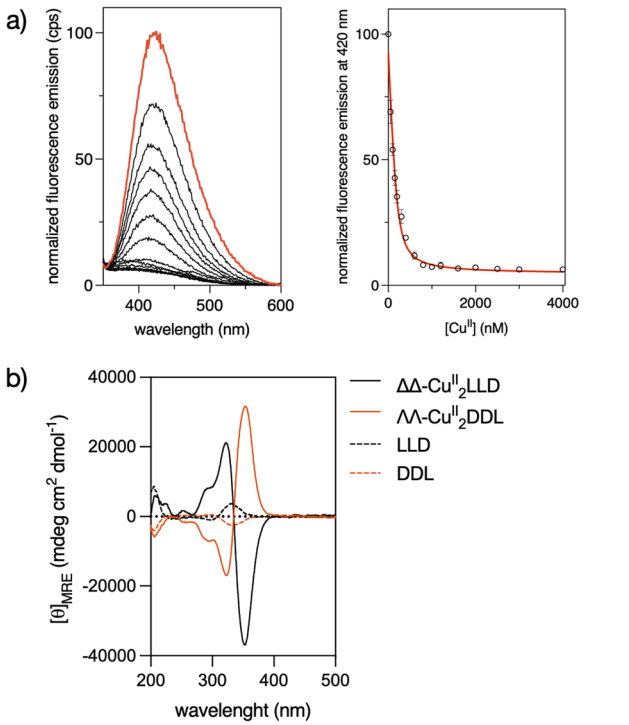

Fig. 1 (a) (Left) Normalized emission spectrum of a 200 nM solution of **LLD** in phosphate buffer (1 mM, NaCl 10 mM, pH 7.0, orange line), and spectra of the same solution in the presence of increasing concentrations of Cu^{II} ions (black lines). (Right) Titration profile of three independent fluorometric titration experiments at 420 nm and best fit according to the 1 : 2 model in DynaFit (same range as main plot). λ_{exc} = 308 nm. (b) CD spectra of 5 μM solutions of **LLD** (black dashed line) and **DDL** (orange dashed line) ligands in phosphate buffer (1 mM, 10 mM NaCl, pH 7.0), and in the presence of 25 μM Cu^{II} ions (same colours, continuous lines).

Circular Dichroism studies revealed a spectrum for the **LLD** peptide ligand that was dominated by a positive Cotton effect band at *ca.* 320 nm. This indicated an important preorganization of the peptide chain and the effective chiral induction of the heterochiral β-turn loops in combination with π-stacking interactions between the bipyridine units. Interestingly, the addition of Cu^{II} ions to a solution of **LLD** resulted in an inverted Cotton effect at this wavelength, accompanied with a large increase in its intensity. This is consistent with the formation of a ΔΔ- (or P) helicate (Fig. 1b). Surprisingly, this is the opposite chirality to that induced by Fe^{II} ions with the same **LLD** peptide ligand, which induce the formation of the diasteromeric (M) helicate.[50] We also synthesised the isomeric **Cu^{II}_2DDL** peptide helicate (Scheme 1), which, as expected, showed a mirror image CD spectrum to that of **Cu^{II}_2LLD**, consistent with a ΛΛ configuration of the Cu^{II} metallopeptide (*i.e.*, with the formation of a M helicate) (Fig. 1b).

It is known that the d^9 configuration of Cu^{II} complexes results in pronounced Jahn–Teller distortion for six-coordinate systems and subsequent kinetic lability of axial ligands, even in chelated systems.[51,52] It appears that the differences in the coordination behavior of Fe^{II} and Cu^{II} lead to different arrangements of the peptide ligand around the metal centres, leading to opposite helical chirality in the corresponding peptide helicates. To better define the coordination of Cu^{II} ions in the helicates, we performed EPR spectra at low (120 K) and room temperature (300 K) using a 200 μM solution of **ΔΔ-Cu^{II}_2LLD** in phosphate buffer (Fig. S6†). At low temperature (*i.e.*, frozen solution), the metallo-peptide spectra displayed a relatively symmetric signal, with an isotropic $g = 2.197$ that suggests regular coordination, indicative of octahedral or trigonal prismatic environments. In contrast, at room temperature, the narrowing of the lines suggests a possible rhombic distortion (Fig. S6†), as observed in other Cu^{II} trisbidentate octahedral complexes due to Jahn–Teller distortion.[53]

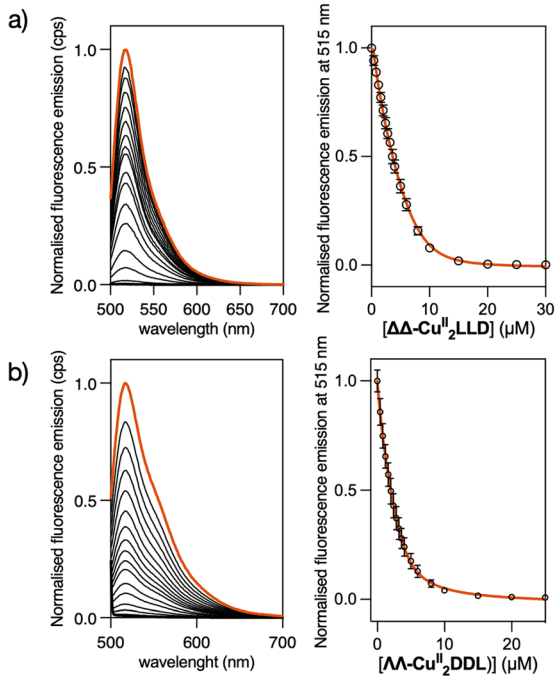

Fig. 2 (a) (Left) Emission spectra of a 2 μM solution of the fluorescein-labelled 3WJ (Flu-3WJ) in absence (orange line) and in the presence of increasing concentrations of **ΔΔ-Cu^{II}_2LLD** (black lines of decreasing intensity). (Right) Profile of the titration with the best fit (orange line) according to a 1 : 1 model plus unspecific interaction in DynaFit, with an apparent $K_D = 260$ nM. (b) (Left) Emission spectra of a 2 μM solution of Flu-3WJ in absence and in the presence of increasing concentrations of **ΛΛ-Cu^{II}_2DDL** (decreasing intensity). (Right) Profile of the titration with the best fit (orange line) according to a 1 : 1 model plus unspecific interaction in DynaFit, with an apparent $K_D = 654$ nM. Conditions: 1 mM phosphate buffer, 10 mM NaCl, pH 7.0, $\lambda_{exc} = 490$ nm.

Cu^{II} peptide helicates recognize three-way DNA junctions *in vitro*

To study the DNA binding properties of the new Cu^{II} peptide helicates, we used a fluorescein-labelled 3WJ (Flu-3WJ; see ESI† Section 2.1 for DNA sequences) and measured its emission in the presence of increasing concentrations of the preformed **ΔΔ-Cu^{II}_2LLD** or **ΛΛ-Cu^{II}_2DDL** helicates. The progressive quenching of the fluorescein emission at 515 nm could be fitted to a 1 : 1 binding mode (Flu-3WJ/helicate) plus nonspecific interactions, with an apparent dissociation constant $K_D = 260$ nM for **ΔΔ-Cu^{II}_2LLD** and $K_D = 654$ nM for **ΔΔ-Cu^{II}_2DDL** (Fig. 2). This indicates that the P helicate, **ΔΔ-Cu^{II}_2LLD**, has higher affinity for the 3WJ. We also attempted to investigate the K_D of the interaction of **ΔΔ-Cu^{II}_2LLD** with fluorescein-labelled dsDNA (Flu-dsDNA), but the mixture precipitated during the titration, which suggests a nonspecific interaction between the peptide helicate and dsDNA.

To ensure that the **ΔΔ-Cu^{II}_2LLD** could bind with 3WJs of different sequence compositions (*i.e.* different GC content) the fluorescein emission assay was repeated with a GC-rich 3WJ sequence (Flu-GC-3WJ, see ESI Section 2.1† for DNA sequences). A K_D of 300 nM was obtained for the interaction between **ΔΔ-Cu^{II}_2LLD** and Flu-GC-3WJ (Fig. S7†), which indicates that the affinity of this Cu^{II} peptide helicate for 3WJs is not limited to a single DNA sequence. The key role played by metal ions in the recognition of 3WJ by these family of peptide helicates was demonstrated in our previous work. There, we demonstrated by means of fluorescence anisotropy experiments the absence of interaction between the free peptide ligand **LLD** and 3WJ.[50]

Kinetic inertness of the ΔΔ-Cu^{II} peptide helicate

Next, we investigated the stability of Cu^{II} peptide helicate in solution, through a competitive binding assay with EDTA—an organic ligand that readily forms complexes with copper ions with extraordinary thermodynamic stability.[54] Specifically, five equivalents of Cu^{II} ions were added to a 2 μM solution of **LLD** ligand, and fluorescence spectra were recorded before and after the addition of the metal ions, that is, before and after the assembly of the peptide helicate **ΔΔ-Cu^{II}_2LLD**. Then, two equivalents of EDTA (with respect to the **LLD** peptide ligand) were added and the fluorescence spectra were recorded for

60 min. The experiment was repeated in the presence of 3WJ. It is necessary to clarify that the peptide ligand **LLD** is able to coordinate two Cu^{II} ions while the EDTA molecule is only able to coordinate a single metal ion, so to perform this classical competition study the stoichiometric ratio between the two ligands must be 1 : 2 (**LLD** : EDTA) against a fixed amount of Cu^{II} ions. The data obtained showed that the ligand substitution reaction takes ≥5 minutes to occur in the absence of 3WJ, but it slows to ≥20 minutes in the presence of 3WJ, which indicates that **ΔΔ-Cu^{II}$_2$LLD** possesses, in addition to its high thermodynamic stability, a remarkable kinetic inertness in water media and probably also *in cellulo* (Fig. S8†).

Analysis of three-way DNA junction recognition of the ΔΔ-Cu^{II} peptide helicate by PAGE

To further analyse the interaction of **ΔΔ-Cu^{II}$_2$LLD** with 3WJ and dsDNA, we performed polyacrylamide gel electrophoresis (PAGE) experiments (Fig. 3a).[55–57] In agreement with the fluorescence studies, we observed that incubation of 3WJ with increasing concentrations of preformed **ΔΔ-Cu^{II}$_2$LLD** resulted in the appearance of a slower-migrating band consistent with the formation of the 3WJ/**ΔΔ-Cu^{II}$_2$LLD** adduct (Fig. 3b). Here, almost all the 3WJ has been complexed with **ΔΔ-Cu^{II}$_2$LLD**, even at the lowest concentration of helicate tested, which is expected for a high-affinity interaction. The intensity of this 3WJ band increases with the concentration of the Cu^{II} helicate (Fig. S9†), while the intensity of the single-stranded DNA band decreases. In contrast, no changes in the position or intensity of the dsDNA were observed upon incubation of the preformed **ΔΔ-Cu^{II}$_2$LLD** helicate with dsDNA in the presence of 3WJ, confirming the low affinity this metallopeptide has for canonical dsDNA (Fig. 3b).

The ΔΔ-Cu^{II} peptide helicate selectively cleaves three-way DNA junctions *in vitro*

To provide further clarity on 3WJ formation and enable ease of visualisation of target 3WJ and off-target dsDNA, PAGE experiments were also performed with fluorophore labelled sequences (Fig. 4a).[58] 3WJ strands were labelled at their 5′ end with FAM, ROX or Cy5, while the dsDNA strands were labelled with FAM and Cy5. Fluorophore 3WJ and dsDNA strands were then incubated with **ΔΔ-Cu^{II}$_2$LLD** and visualised using a multiplex fluorescent assay (Fig. 4a). The blue (FAM), green (ROX) and red (Cy5) signal of the 3WJ sequences were combined to produce a yellow 3WJ band, while the blue (FAM) and red (Cy5) dsDNA strands appear pink. This multiplex binding assay was next applied for the analysis of the cleavage profile of **ΔΔ-Cu^{II}$_2$LLD**.

The ability of **ΔΔ-Cu^{II}$_2$LLD** to selectively recognise and cleave 3WJs *in vitro* was analysed by PAGE (Fig. 4b). The fluorescently labelled target 3WJ and off-target dsDNA oligos (see

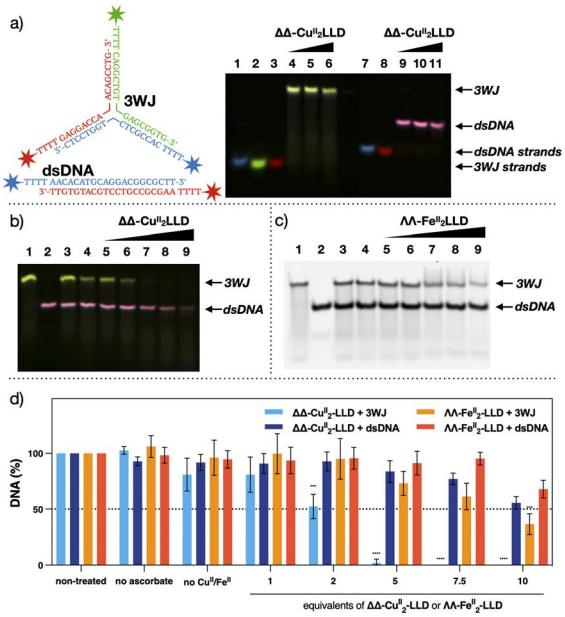

Fig. 4 (a) Fluorescently labelled target 3WJ and off-target dsDNA. Blue = FAM, Green = ROX and Red = Cy5 (see ESI Section 2.3† for DNA sequences and experimental conditions). Multiplex image from 20% native analysis of the formation of 3WJ in the presence of increasing concentrations of **ΔΔ-Cu^{II}$_2$LLD**. Lane 1: FAM-labelled single strand (ss) of 3WJ. Lane 2: ROX-labelled ss. Lane 3: Cy5-labelled ss of 3WJ. Lane 4–6: 3WJ strands incubated with 1, 2 or 3 eq. of **ΔΔ-Cu^{II}$_2$LLD**, respectively. Lane 7: FAM-labelled ss of dsDNA. Lane 8: Cy5-labelled ss of dsDNA. Lanes 9–11: dsDNA incubated with 1, 2 or 3 eq. of **ΔΔ-Cu^{II}$_2$LLD**, respectively. See Fig. S10† for individual images from multiplex assay. (b) PAGE analysis of the DNA damage inflicted by **ΔΔ-Cu^{II}$_2$LLD**. Fluorophore labelled DNA was utilised to ensure clarity of target 3WJ DNA (yellow) and off-target dsDNA (pink). Lane 1: 3WJ. Lane 2; dsDNA. Lane 3: 3WJ and dsDNA incubated with **ΔΔ-Cu^{II}$_2$LLD**. Lane 4: Target and off-target with **LLD** peptide ligand (no Cu^{II} present). Lanes 5–9: 3WJ and dsDNA incubated with 1, 2, 5, 7.5 or 10 eq. of **ΔΔ-Cu^{II}$_2$LLD** and Na-L-ascorbate (10 eq. to **ΔΔ-Cu^{II}$_2$LLD**). Individual images available in Fig. S11.† (c) Control cleavage experiment performed with **ΛΛ-Fe^{II}$_2$LLD**. Lane 1: 3WJ DNA. Lane 2: dsDNA off-target. Lane 3; control of 3WJ and dsDNA incubated with **ΛΛ-Fe^{II}$_2$LLD**. Lane 4: 3WJ and dsDNA with non-metalated **LLD** peptide ligand. Lanes 5–9: 3WJ and dsDNA incubated with 1, 2, 5, 7.5 or 10 eq. of **ΛΛ-Fe^{II}$_2$LLD** and Na-L-ascorbate (10 eq. to **ΛΛ-Fe^{II}$_2$LLD**). (d) Band densitometry analysis of cleavage induced upon 3WJ and dsDNA by **ΔΔ-Cu^{II}$_2$LLD** (Fig. S12†) and **ΛΛ-Fe^{II}$_2$LLD** (Fig. 4c and S13†). * = $P \leq 0.05$ ** = $P \leq 0.01$ *** = $P \leq 0.001$ and **** = $P \leq 0.0001$. Na-L-ascorbate concentration is 10 eq. to **ΔΔ-Cu^{II}$_2$LLD** or **ΛΛ-Fe^{II}$_2$LLD**.

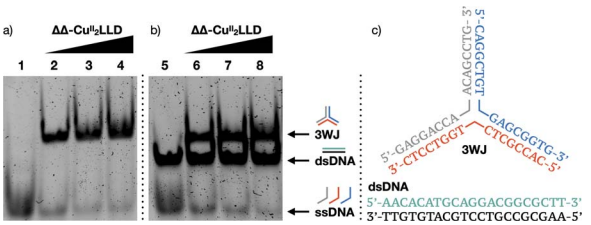

Fig. 3 (a) 10% native PAGE analysis of 3WJ strands in the absence (lane 1) and presence 1, 2 and 3 equivalents of **ΔΔ-Cu^{II}$_2$LLD** (lanes 2–4); (b) 3WJ strands and dsDNA in the absence (lane 5) and presence of **ΔΔ-Cu^{II}$_2$LLD** (1–3 eq. in lanes 6–8, respectively). 3WJ remains as single-stranded DNA in the absence of **ΔΔ-Cu^{II}$_2$LLD** and forms the 3WJ when **ΔΔ-Cu^{II}$_2$LLD** is present. In contrast, dsDNA can be visualised in lanes 5–8 and remains unchanged in the presence of increasing concentrations of the Cu^{II} peptide helicate, demonstrating the low affinity of the metallopeptide for canonical DNA; (c) 3WJ and dsDNA sequences used for PAGE analysis.

ESI 2.3† for DNA sequences) were incubated with increasing equivalents **ΔΔ-Cu$^{II}_2$LLD** and Na-L-ascorbate at 37 °C for 24 hours. PAGE analysis revealed that the Cu^{II} peptide helicate selectively cleaves 3WJ, which fully disappears when exposed to 5 eq. of **ΔΔ-Cu$^{II}_2$LLD**, while the dsDNA present in the sample remains intact when exposed up to 7.5 equivalents of the Cu^{II} peptide helicate. A control cleavage experiment was also performed with **ΛΛ-Fe$^{II}_2$LLD**. Here, 3WJ and dsDNA were incubated with the Fe^{II} helicate and Na-L-ascorbate under identical conditions to that of the **ΔΔ-Cu$^{II}_2$LLD** assay, and the cleavage profile was visualised by PAGE (Fig. 4c). Band densitometry revealed a significant difference between the cleavage **ΔΔ-Cu$^{II}_2$LLD** induced towards 3WJ compared to the off-target dsDNA; for example, just 2% of the 3WJ remained *versus* 80% of off-target dsDNA following exposure to 5 eq. of **ΔΔ-Cu$^{II}_2$LLD** (Fig. 4d and S14†). By contrast, **ΛΛ-Fe$^{II}_2$LLD** did not show selectivity in the cleavage of 3WJ *versus* dsDNA across all tested concentrations (Fig. 4d and S14†). Moreover, the Fe^{II} peptide helicate is only able to cleave 70% of 3WJ at the highest concentration of metallopeptide tested (10 eq.), which highlights its lack of efficiency.

A time point study was performed to determine the incubation period required to achieve 3WJ selective damage (Fig. S14†). This revealed that cleavage initiates within 1 hour and increases up to 12 hours; from 12 to 24 hours no significant increase in cleavage was observed. This indicates that **ΔΔ-Cu$^{II}_2$LLD** can rapidly and selectively damage DNA 3WJs, and that off-target dsDNA damage would not be expected upon longer incubation. Combining the results of Fig. 3, 4 and S10–S15,† it can be concluded that **ΔΔ-Cu$^{II}_2$LLD** can discriminate with great efficiency between 3WJ and dsDNA, and selectively cleave 3WJ in the presence of canonical DNA. To our knowledge, this is the first example of such activity for a chemical nuclease *in vitro*.

Next, the cleavage mechanism for the **ΔΔ-Cu$^{II}_2$LLD** helicate was investigated using reactive oxygen species (ROS) scavengers.[59,60] Here, 3WJ was incubated with **ΔΔ-Cu$^{II}_2$LLD**, Na-L-ascorbate, and a series of selective ROS scavengers (L-histidine, D-mannitol, L-methionine, and tiron (sodium catechol sulfate)), and the resulting cleavage profiles were visualized by PAGE (Fig. 5). The presence of tiron significantly impeded the activity of the peptide helicate, indicating that superoxide radicals ($O_2^{\bullet-}$)[61] play a dominant role in the 3WJ cleavage inflicted by **ΔΔ-Cu$^{II}_2$LLD**. To probe this finding further, we determined if diffusible superoxide radicals were directly contributing to DNA cleavage by examining the activity in the presence of 4-hydroxy-TEMPO, a known scavenger of difussible $O_2^{\bullet-}$ (Fig. S16†).[62] TEMPO resulted in negligible cleavage inhibition indicating that difussible $O_2^{\bullet-}$ plays a minimal role in **ΔΔ-Cu$^{II}_2$LLD** cleavage and that, instead, oxidative damage is likely mediated by a copper bound superoxo radical species (Cu–$O_2^{\bullet-}$) proximate to the 3WJ. The scavenger L-histidine also impeded 3WJ damage, which suggested that singlet oxygen ($^1O_2$) is contributing to the cleavage mechanism. However, since $^1O_2$ is usually generated under photoactivated conditions we further investigated the role of this ROS in **ΔΔ-Cu$^{II}_2$LLD** activity. The scavenger assay was therefore expanded to include deuterium oxide (D_2O)—a known $^1O_2$ stabiliser—and sodium azide (NaN_3)—a known scavenger of $^1O_2$ (Fig. 5a). The presence of D_2O and NaN_3 did not perturb 3WJ cleavage and consequently it is not clear at this point how $^1O_2$ mediates **ΔΔ-Cu$^{II}_2$LLD** activity. It should be noted that several recent studies reporting the dsDNA damaging effects of polynuclear Cu^{II} metallonucleases have predicted $^1O_2$-mediated DNA damage and identified L-histidine as viable scavenger *in vitro* and *in cellulo*.[63,64]

A rhodamine-labelled ΔΔ-Cu^{II} peptide helicate selective labels DNA-replication sites in mammalian cells

To this point we have demonstrated that the **ΔΔ-Cu$^{II}_2$LLD** readily forms in solution, its stability in aqueous environments, and that **ΔΔ-Cu$^{II}_2$LLD** can selectively bind and damage 3WJ *in vitro*. Next, *in cellulo* studies were performed to investigate the ability of the Cu^{II} helicate to selectively target DNA replication centres (*i.e.*, 3WJs in the cell nuclei). Preliminary experiments indicated, as was the case with Fe^{II} analogues,[50] that a TAMRA-labelled Cu^{II} peptide helicate, **ΔΔ-Cu$^{II}_2$TAMRA-LLD** (Fig. S2†), did not internalise in Vero cells. However, it readily translocated in digitonin-treated cells where it showed a diffused

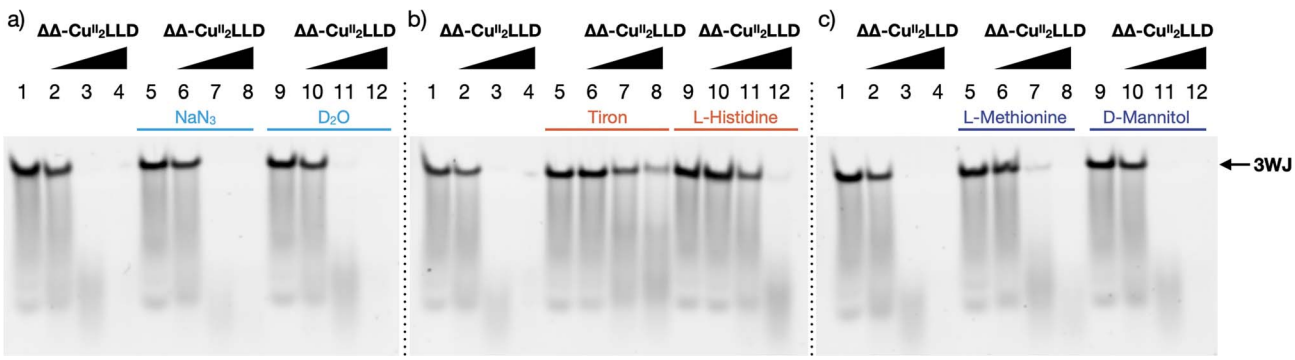

Fig. 5 20% native PAGE showing the cleavage profile of the **ΔΔ-Cu$^{II}_2$LLD** in the presence of ROS scavengers: (a) NaN_3 and D_2O; (b) tiron and L-histidine; (c) L-methionine and D-mannitol. Lane 1–4: control (no scavenger). Lanes 5–8: (a) NaN_3; (b) tiron; (c) L-methionine. Lanes 9–12: (a) D_2O; (b) L-histidine; (c) D-mannitol. Lanes 1, 5, 9: 3WJ control. Lanes 2, 6, 10: 1 eq. **ΔΔ-Cu$^{II}_2$LLD**. Lanes 3, 7, 11: 5 eq. **ΔΔ-Cu$^{II}_2$LLD**. Lanes 4, 8, 12: 10 eq. **ΔΔ-Cu$^{II}_2$LLD**. All lanes (excluding controls) contain Na-L-ascorbate (10 eq. to **ΔΔ-Cu$^{II}_2$LLD**).

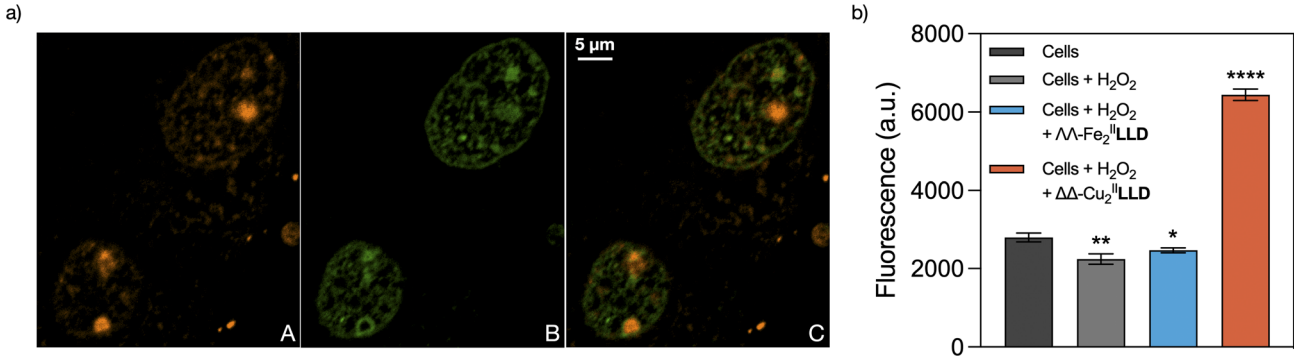

Fig. 6 (a) **ΔΔ-Cu$^{II}_2$TAMRA-LLD** selectively stains DNA replication sites at the cell nuclei. Vero cells expressing protein GFP-PCNAL2 were incubated in the presence of 25 μg mL^{-1} of digitonin for 3 min and then in the presence of 5 μM of **ΔΔ-Cu$^{II}_2$TAMRA-LLD** for 15 min. The Cu^{II} peptide helicate used in these studies was previously assembled before the internalization experiment by adding 5 eq. of $CuCl_2 \cdot 2H_2O$ to an aqueous solution of **TAMRA-LLD** peptide ligand. (A) Red channel emission showing the distribution of the TAMRA-labelled helicate; (B) green channel, corresponding to the emission of the GFP-PCNAL2 probe that labels DNA replication foci; (C) overlay of the green and red channels, which shows that **ΔΔ-Cu$^{II}_2$TAMRA-LLD** has localised at the replication foci. Nucleoli are clearly labelled as red spots inside the cell nuclei. The images show a representative confocal section of the Vero cells. (b) Detection of free DNA ends by TUNEL assay. S-phase synchronized Vero cells were incubated with H_2O_2 alone and with **ΛΛ-Fe$^{II}_2$LLD** or **ΔΔ-Cu$^{II}_2$LLD** plus H_2O_2 at 37 °C for 2 hours and then subjected to TUNEL analysis for the detection of free DNA ends. Results are represented as the mean with standard deviation of a triplicate experiment * = $P \leq 0.05$ ** = $P \leq 0.01$ *** = $P \leq 0.001$ and **** = $P \leq 0.0001$.

distribution in the cytosol, and a strong punctuated distribution in the nucleus, as well as an evident concentration in the nucleolus (Fig. 6a(A)—red and Fig. S18†). Most of the nuclear spots co-localized with GFP-tagged Proliferating Nuclear Antigen (PCNA), which specifically labels DNA replication foci in actively dividing cells (Fig. 6a(B)—green).[65] While its cytosolic distribution and association with the nucleoli might reflect some off-target RNA-binding of the helicate, replisomes labelled by PCNA are enriched in 3WJs due to the presence of replication forks. Thus, our results strongly suggest the direct association of the Cu^{II} peptide helicate with 3WJs structures in functional cell nuclei. Moreover, control experiments show that the free **LLD** peptide ligand does not localise in the DNA replication centres (Fig. S17†). As already suggested by the results obtained in the competition studies with EDTA described above, this control experiment further demonstrates that the **ΔΔ-Cu$^{II}_2$LLD** helicate is stable in cell medium and that it only binds DNA replication centres in the nucleus as a discrete metallopeptide.

The ΔΔ-Cu^{II} peptide helicate selective cleaves DNA-replication foci in mammalian cells

Having demonstrated that **ΔΔ-Cu$^{II}_2$LLD** is stable *in cellulo* and associates with 3WJ-enriched foci in cellular DNA, we next investigated if it could exert its nuclease activity upon chromatin-associated 3WJs in cells. To maximize the number of cells undergoing DNA replication, and thus increase the chances of detecting free DNA ends obtained by nuclease cleavage of 3WJs, we used Vero cells that were previously synchronised by 42 h of serum deprivation.[66] 16 h after re-supplementation of the cultures with 10% serum—when most of the cells were in S phase—the cells were pre-treated with digitonin and then incubated with H_2O_2 in the presence or absence of **ΔΔ-Cu$^{II}_2$-LLD**. Cells were then incubated for 2 h at 37 °C and subjected to a Terminal deoxynucleotidyl transferase (TdT) dUTP Nick-End Labelling (TUNEL) assay. The TUNEL assay uses TdT polymerase to label the free ends of DNA with a fluorescent dUTP, and thereby enables detection of cleavage sites. Here, the free DNA ends in the cell nuclei DNA (*i.e.*, DNA sites cleaved by **ΔΔ-Cu$^{II}_2$LLD**) were detected through Alexa Fluor 488™ fluorescence.[67] Very importantly, the results show that incubation of **ΔΔ-Cu$^{II}_2$LLD** in the presence of H_2O_2 produced a significant increase for the TUNEL fluorescent signal (Fig. 6b), which indicates the presence of free DNA ends and thus, nuclease activity *in cellulo*. A control experiment was also performed with **ΛΛ-Fe$^{II}_2$LLD** in the presence of H_2O_2. Significantly, the increase in fluorescent signal—indicative of DNA cleavage—was not observed for the Fe^{II} helicate, which agrees with the above-described *in vitro* studies, which suggested a lack of nuclease activity. To our knowledge, this is the first example of such activity for a chemical nuclease *in cellulo*.

Conclusion

We reported herein the synthesis of two new chiral dinuclear oligocationic Cu^{II} peptide helicates derived from two enantiomeric peptide ligands equipped with six chelating 2,2′-bipyridine residues, named **LLD** and **DDL**, following a SPPS methodology.[50] Spectrofluorimetric and PAGE DNA binding studies indicate that both Cu^{II} peptide helicates can recognize 3WJs *in vitro* with high affinity and selectivity, even in the presence of canonical DNA, showing chiral discrimination between the two diastereoisomers, being **ΔΔ-Cu$^{II}_2$LLD** the metallopeptide with higher 3WJ affinity of the two (K_D = 260 nm *vs.* 654 nm). Moreover, the kinetic inertness of **ΔΔ-Cu$^{II}_2$LLD** in water was investigated through a competition study with EDTA in presence and absence of 3WJ, suggesting that **ΔΔ-Cu$^{II}_2$LLD** is very stable *in vitro* and *in cellulo*.

The studies carried out clearly show that **ΔΔ-Cu$^{II}_2$LLD** is an efficient and selective *in vitro* agent for the cleavage of 3WJs, even in the presence of canonical DNA. The mechanism through which this 3WJ cleavage by **ΔΔ-Cu$^{II}_2$LLD** occurred was also investigated. Studies using ROS scavengers showed that metal-bound superoxide radicals (Cu–$O_2^{\bullet-}$) play the key role in the cleavage process and suggest that singlet oxygen ($^1O_2$) is also involved in some way.

The ability **ΔΔ-Cu$^{II}_2$LLD** to internalise in cells was studied using of Cu^{II} helicate labelled with TAMRA (**ΔΔ-Cu$^{II}_2$TAMRA-LLD**). This helicate was effectively internalised by digitonin-treated mammalian cells and was localised into the nucleus. Its nuclear distribution matched the localization of DNA replication sites, demonstrating that **ΔΔ-Cu$^{II}_2$LLD** binds with high affinity and selectivity to 3WJ *in cellulo*. Finally, the selective cleavage of DNA replication foci in cells was evaluated by TUNEL assay. The studies performed indicate that **ΔΔ-Cu$^{II}_2$LLD** produced a significant increase of the TUNEL fluorescent signal in the presence of H_2O_2, which indicates the presence of free DNA ends and thus, nuclease activity *in cellulo*.

To our knowledge, **ΔΔ-Cu$^{II}_2$LLD** is the first example of a chemical nuclease that selectively cleaves 3WJ both *in vitro* and *in cellulo*. As DNA replication is deregulated in cancer cells, we strongly believe that this work will form the basis of a new class of anticancer metallodrug that target and damage with high efficiency and selectivity this noncanonical DNA structure that is transiently generated in the DNA replication foci of cell nuclei.

Data availability

Raw data for Fig. 1–6 are published in the figshare repository **https://doi.org/10.6084/m9.figshare.22754600**.

Author contributions

M. V. L., J. M.-C. and A. K. conceived and designed the investigations. M. E. V. deeply assisted in the design of the investigations, interpretation of experimental data and proof-reading of the manuscript. A. A.-O., N. B.-P., B. McG. and J. G.-G. performed the experiments. D. B. assisted in conducting DNA-binding studies. F. R. conducted the EPR studies. M. V. L, J. M.-C. and A. K. wrote the manuscript.

Conflicts of interest

There are no conflicts to declare.

Acknowledgements

M. V. L., M. E. V., and J. M.-C. thank grants RTI2018-099877-B-I00, PID2021-127857NB-I00, PID2019-105308RB-I00 and PID2021-127702NB-I00 by MCIN/AEI/10.13039/501100011033 and by ERDF A way of making Europe. M. V. L. thanks Fundación Científica de la Asociación Española Contra el Cáncer (Ideas Semilla 2021 – IDEAS211154VÁZQ). M. V. L, J. M.-C, M. E. V and F. R. thank Xunta de Galicia (grants ED431C 2021/29 and ED431B 2021/13). J. G.-G. thanks the USC and NextGeneration EU program for his Margarita Salas postdoc fellowship. A. A.-O thanks the Spanish Ministry of Science and Innovation/Spanish Research Agency for her FPI fellowship. A. K. and B. McG. acknowledge funding from the Irish Research Council (EPSPD/2022/164 and IRCLA/2022/3815), Science Foundation Ireland funded research centers SSPC and CÚRAM (12/RC/2275 P2), and the European Union's Horizon 2020 Research and Innovation Program under the Marie Skłodowska-Curie grant agreement No. 861381.

Notes and references

1 R. A. Alderden, M. D. Hall and T. W. J. Hambley, The discovery and development of cisplatin, *J. Chem. Educ.*, 2006, **83**, 728–734.
2 E. J. Anthony, E. M. Bolinho, H. E. Bridgewater, O. W. L. Carter, J. M. Donnely, C. Imberti, E. C. Lant, F. Lermyte, R. J. Needham, M. Palau, P. J. Sadler, H. Shi, F.-X. Wang, W.-Y. Zhang and Z. Zhang, Metallodrugs are unique: opportunities and challenges of discovery and development, *Chem. Sci.*, 2020, **11**, 12888–12917.
3 A. Shivaligam, M. A. Izquierdo, A. L. Marois, A. Vysniauskas, K. Suhling, M. K. Kuimova and R. Vilar, The interactions between a small molecule and G-quadruplexes are visualized by fluorescence lifetime imaging microscopy, *Nat. Commun.*, 2015, **6**, 8178.
4 R. Vilar, Interaction of metal complexes with G-quadruplex DNA, *Adv. Inorg. Chem.*, 2020, **75**, 425–445.
5 D. Bouzada, I. Salvadó, G. Barka, G. Rama, J. Martínez-Costas, R. Lorca, A. Somoza, M. Melle-Franco, M. E. Vázquez and M. Vázquez López, Selective G-quadruplex binding by oligoarginine-Ru(dppz) metallopeptides, *Chem. Commun.*, 2018, **54**, 658–661.
6 A. Oleksi, A. G. Blanco, R. Boer, I. Usón, J. Aymamí, A. Rodger, M. J. Hannon and M. Coll, Molecular recognition of a three-way DNA junction by a metallosupramolecular helicate, *Angew. Chem., Int. Ed.*, 2006, **45**, 1227–1231.
7 C. A. J. Hooper, L. Cardo, J. S. Craig, L. Melidis, A. Garai, R. T. Egan, V. Sadovnikova, F. Burkert, L. Male, N. J. Hodges, D. D. F. Browning, R. Rosas, F. Liu, F. V. Rocha, M. A. Lima, S. Liu, D. Bardelang and M. J. Hannon, Rotaxanating metallo-supramolecular nanocylinder helicates to switch DNA junction binding, *J. Am. Chem. Soc.*, 2020, **142**, 20651–20660.
8 A. D. Faulkner, R. A. Kaner, Q. M. A. Abdallah, G. Clarkson, D. J. Fox, P. Gurnani, S. E. Howson, R. M. Phillips, D. I. Roper, D. H. Simpson and P. Scott, Asymmetric triplex metallohelices with high and selective activity against cancer cells, *Nat. Chem.*, 2014, **6**, 797–803.
9 H. Song, S. A. Allison, V. Brabec, H. E. Bridgewater, J. Kasparkova, H. Jostrhunova, V. Novohradsky, R. M. Phillips, J. Pracharova, N. J. Rogers, S. L. Shepherd and P. Scott, Glycoconjugated metallohelices have improved nuclear delivery and suppress tumour growth *in vivo*, *Angew. Chem., Int. Ed.*, 2020, **59**, 14677–14685.

10 J. Gómez-González, D. Bouzada, L. A. Pérez-Márquez, G. Sciortino, J.-D. Maréchal, M. Vázquez López and M. E. Vázquez, Stereoselective self-assembly of DNA binding helicates directed by the viral β-annulus trimeric peptide motif, *Bioconjugate Chem.*, 2021, **32**, 1564–1569.
11 J. Gómez-González, D. G. Peña, G. Barka, G. Sciortino, J.-D. Maréchal, M. Vázquez López and M. E. Vázquez, Directed self-assembly of trimeric DNA-binding chiral miniprotein helicates, *Front. Chem.*, 2018, **6**, 520.
12 I. Gamba, G. Rama, E. Ortega-Carrasco, J.-D. Maréchal, J. Martínez-Costas, M. E. Vázquez and M. Vázquez López, Programmed stereoselective assembly of DNA-binding helical metallopeptides, *Chem. Commun.*, 2014, **50**, 11097–11100.
13 J. S. Craig, L. Melidis, H. D. Williams, S. J. Dettmer, A. A. Heidecker, P. J. Altmann, S. Guan, C. Campbell, D. F. Browning, R. K. O. Sigel, S. Johannsen, R. T. Egan, B. Aikman, A. Casini, A. Pöthig and M. J. Hannon, Organometallic pillarplexes that bind DNA 4-way Holliday junctions and forks, *J. Am. Chem. Soc.*, 2023, **145**, 13570–13580.
14 K. J. Neelsen and M. Lopes, Replication fork reversal in eukaryotes: from dead end to dynamic response, *Nat. Rev. Mol. Cell Biol.*, 2015, **16**, 207–220.
15 K. C. Woods, S. S. Martin, V. C. Chu and E. P. Baldwin, Quasi-equivalence in site-specific recombinase structure and function: crystal structure and activity of trimeric Cre recombinase bound to a three-way Lox DNA junction, *J. Mol. Biol.*, 2001, **313**, 49–69.
16 S. A. Barros and D. M. Chenoweth, Recognition of nucleic acid junctions using triptycene-based molecules, *Angew Chem. Int. Ed. Engl.*, 2014, **53**, 13746–13750.
17 J. Novotna, A. Laguerre, A. Granzhan, M. Pirrotta, M.-P. Teulade-Fichou and D. Monchaud, Cationic azacryptands as selective three-way DNA junctions binding agents, *Org. Biomol. Chem.*, 2015, **13**, 215–222.
18 J. Zhu, C. J. E. Haynes, M. Kieffer, J. L. Greenfield, R. D. Greenhalgh, J. R. Nitschke and U. F. Keyser, $Fe^{II}_4L_4$ tetrahedron binds to nonpaired DNA bases, *J. Am. Chem. Soc.*, 2019, **141**, 11358–11362.
19 J. Gómez-González, L. Martínez-Castro, J. Tolosa-Barrilero, A. Alcalde, S. Learte-Aymami, J. L. Mascareñas, J. C. García-Martínez, J. Martínez-Costas, J. D. Maréchal, M. Vázquez López and M. E. Vázquez, Selective recognition of A/T-rich DNA 3-way junctions with a three-fold symmetric tripeptide, *Chem. Commun.*, 2022, **58**, 7769–7772.
20 J. Atkinson and P. McGlynn, Replication fork reversal and the maintenance of genome stability, *Nucleic Acid Res.*, 2009, **37**, 3475–3492.
21 L. S. Shlyakhtenko, V. N. Potaman, R. R. Sinden, A. A. Gall and Y. L. Lyubchenko, Structure and dynamics of three-way DNA junctions: atomic force microscopy studies, *Nucleic Acid Res.*, 2000, **28**, 3472–3477.
22 R. R. Sinden, M. J. Pytlos-Sinden and V. N. Potaman, Slipped strand DNA structures, *Front. Biosci.*, 2007, **12**, 4788–4799.
23 C.-H. Hu, F.-Y. Xu, K. Wang, A. N. Pearson and G. D. Pearson, Symmetrical adenovirus minichromosomes have hairpin replication intermediates, *Gene*, 1992, **110**, 145–150.
24 H. Liao, F. Ji, T. Helleday and S. Ying, Mechanisms for stalled replication fork stabilization: new targets for synthetic lethality strategies in cancer treatments, *EMBO Rep.*, 2008, **19**, e46263, DOI: **10.15252/embr.201846263**.
25 K. Duskova, P. Lejault, É. Penchimol, R. Guillot, S. Britton, A. Granzhan and D. Monchaud, DNA junction ligands trigger DNA damage and are synthetic lethal with DNA repair inhibitors in cancer cells, *J. Am. Chem. Soc.*, 2020, **142**, 424–435.
26 A. Bacolla and R. D. Wells, Non-B DNA conformations as determinants of mutagenesis and human disease, *Mol. Carcinog.*, 2009, **48**, 273–285.
27 R. D. Wells, Non-B DNA conformations, mutagenesis and disease, *Trends Biochem. Sci.*, 2007, **32**, 271–278.
28 H. Tateishi-Karimata and N. Sugimoto, Roles of non-canonical structures of nucleic acids in cancer and neurodegenerative diseases, *Nucleic Acid Res.*, 2021, **49**, 7839–7855.
29 J. Zell, F. R. Sperti, S. Britton and D. Monchaud, DNA folds threaten genetic stability and can be leveraged for chemotherapy, *RSC Chem. Biol.*, 2021, **2**, 47–76.
30 H. Tateishi-Karimata and N. Sugimoto, Chemical biology of non-canonical structures of nucleic acids for therapeutic applications, *Chem. Commun.*, 2020, **56**, 2379–2390.
31 L. A. Howell and M. Searcey, Targeting higher-order DNA: beyond the G-quadruplex, *ChemBioChem*, 2009, **10**, 2139–2143.
32 F. Mancin, P. Scrimin, P. Tecilla and U. Tonellato, Artificial metallonucleases, *Chem. Commun.*, 2005, 2540–2548.
33 L. J. Childs, J. Malina, B. E. Rolfsnes, M. Pascu, M. J. Prieto, M. J. Broome, P. M. Rodger, E. Sletten, V. Moreno, A. Rodger and M. J. Hannon, A DNA-binding copper(I) metallosupramolecular cylinder that acts as an artificial nuclease, *Chem.–Eur. J.*, 2006, **12**, 4919–4927.
34 Z.-R. Li, J. Li, W. Cai, J. Y. H. Lai, S. M. K. McKinnie, W.-P. Zhang, B. S. Moore, W. Zhang and P.-Y. Qian, Macrocyclic colibactin induces DNA double-strand breaks *via* copper-mediated oxidative cleavage, *Nat. Chem.*, 2019, **11**, 880–889.
35 C. Wen-de, C. Lüdtke and M. Kulak, Copper complexes of N-donor ligands as artificial nucleases, *Eur. J. Inorg. Chem.*, 2014, 2597–2612.
36 N. Z. Fantoni, Z. Molphy, S. O'Carroll, G. Menounou, G. Mitrikas, M. G. Krokidis, C. Chatgiliaglu, J. Colleran, A. Banasiak, M. Clynes, S. Roche, S. Kelly, V. McKee and A. Kellet, Polypyridyl-based copper phenanthrene complexes: combining stability with enhanced DNA recognition, *Chem.–Eur. J.*, 2020, **27**, 971–983.
37 T. J. P. McGivern, S. Afsharpour and C. J. Marmion, Copper complexes as artificial DNA metallonucleases: From Sigman's reagent to next generation anti-cancer agent?, *Inorg. Chim. Acta*, 2018, **472**, 12–39.

38 C. Liu, M. Wang, T. Zhang and H. Sun, DNA hydrolysis promoted by di- and multi-nuclear metal complexes, *Coord. Chem. Rev.*, 2004, **248**, 147–168.

39 K. J. Humphreys, K. D. Karlin and S. E. Kokita, Recognition and strand scission at junctions between single- and double-stranded DNA by a trinuclear copper complex, *J. Am. Chem. Soc.*, 2001, **123**, 5588–5589.

40 P. G. Shultz, J. S. Taylor and P. B. Dervan, Design synthesis of a sequence-specific DNA cleaving molecule. (Distamycin-EDTA)iron(II), *J. Am. Chem. Soc.*, 1982, **104**, 6861–6863.

41 M. Pitié, C. J. Burrows and B. Meunier, Mechanisms of DNA cleavage by copper complexes of 3-Clip-Phen and of its conjugate with a distamycin analogue, *Nucleic Acid Res.*, 2000, **28**, 4856–4864.

42 C. H. B. Chen, A. Mazumber, J. F. Constant and D. S. Sigman, New conjugates with low molecular weight targeting ligands, *Bioconjugate Chem.*, 1993, **4**, 69–77.

43 M. Pitié, A. Croisy, D. Carrez, C. Blodron and B. Meunier, Cytostatic activity of 1,10-phenantroline derivatives generated by the clip-phen strategy, *ChemBioChem*, 2005, **6**, 686–691.

44 A. Zaid, J.-S. Sun, C.-H. Nguyen, E. Bisagni, T. Garestier, D. S. Grierson and R. Zain, Triple-helix directed cleavage of double-stranded DNA by benzoquinoquinozaline-1,10-phenantroline conjugates, *ChemBioChem*, 2004, **5**, 1550–1557.

45 Z. Yu, M. Han and J. Cowan, Toward the design of a catalytic metallodrug: selective cleavage of G-quadruplex telomeric DNA by an anticancer copper-acridine-ATCUN complex, *Angew. Chem., Int. Ed.*, 2015, **54**, 1901–1905.

46 O. Luige, P. P. Bose, R. Stultz, P. Steunenberg, O. Brun, S. Andersson, M. Murtola and R. Strömberg, Zn^{2+}-dependent peptide nucleic acid-based artificial ribonucleases with unprecedent efficiency and specificity, *Chem. Commun.*, 2021, **57**, 10911–10914.

47 B. McGorman, N. Z. Fantoni, S. O'Carroll, A. Ziemele, A. H. El-Sagheer, T. Brown and A. Kellett, Enzymatic synthesis of chemical nuclease triplex-forming oligonucleotides with gene-silencing applications, *Nucleic Acid Res.*, 2020, **50**, 5467–5481.

48 N. Z. Fantoni, B. McGorman, Z. Molphy, D. Singleton, S. Walsh, A. H. El-Sagheer, V. McKee, T. Brown and A. Kellett, Development of gene-targeted polypyridyl triplex-forming oligonucleotide hybrids, *ChemBioChem*, 2020, **21**, 3563–3574.

49 T. Lauria, C. Slator, V. McKee, M. Müller, S. Stazzoni, A. L. Crisp, T. Carell and A. Kellett, A click chemistry approach to developing molecularly targeted DNA scissors, *Chem.–Eur. J.*, 2020, **26**, 16782–16792.

50 J. Gómez-González, Y. Pérez, G. Sciortino, L. Roldan-Martín, J. Martínez-Costas, J.-D. Maréchal, I. Alfonso, M. Vázquez López and M. E. Vázquez, Dynamic stereoselection of peptide helicates and their selective labeling of DNA replication foci in cells, *Angew. Chem., Int. Ed.*, 2021, **60**, 8859–8866.

51 D. H. Powell, L. Helm and A. E. Merbach, ^{17}O nuclear magnetic resonance in aqueous solutions of Cu^{2+}: the combined effect of Jahn–Teller inversion and solvent exchange on relaxation rates, *J. Chem. Phys.*, 1991, **95**, 9258–9265.

52 M. A. Halcrow, Jahn–Teller distortions in transition metal compounds, and their importance in functional molecular and inorganic materials, *Chem. Soc. Rev.*, 2013, **42**, 1784–1795.

53 M. V. Veidis, G. H. Schreiber, T. E. Gough and G. J. Palenik, Jahn–Teller distortions in octahedral copper(II) complexes, *J. Am. Chem. Soc.*, 1969, **91**, 1859–1860.

54 S. Chaberek Jr and A. E. Martell, Interaction of divalent metal Ions with N-hydroxyethylethylenediaminetriacetic acid, *J. Am. Chem. Soc.*, 1955, **77**, 1477–1480.

55 L. M. Hellman and M. G. Fried, Electrophoretic Mobility Shift Assay (EMSA) for detecting protein-nucleic acid interactions, *Nat. Protoc.*, 2007, **2**, 1849–1861.

56 D. Lane, P. Prentki and M. Chandler, Use of gel retardation to analyze protein-nucleic acid interactions, *Microbiol. Rev.*, 1992, **56**, 509–528.

57 R. S. Tuma, M. P. Beaudet, X. Jin, L. J. Jones, C. Y. Cheung, S. Yue and V. L. Singer, Characterization of SYBR gold nucleic acid gel stain: a dye optimized for use with 300-nm ultraviolet transilluminators, *Anal. Biochem.*, 1999, **268**, 278–288.

58 B. McGorman, S. Poole, M. Vázquez López and A. Kellett, Analysis of non-canonical three- and four-way DNA junctions, *Methods*, 2023, **219**, 30–38.

59 A. Kellett, Z. Molphy, C. Slator, V. McKee and N. P. Farrell, Molecular methods for assessment of non-covalent metallodrug–DNA interactions, *Chem. Soc. Rev.*, 2019, **48**, 971–988.

60 B. McGorman, N. Z. Fantoni, S. O'Carroll, A. Ziemele, A. H. El-Sagheer, T. Brown and A. Kellett, Enzymatic synthesis of chemical nuclease triplex-forming oligonucleotides with gene-silencing applications, *Nucleic Acid Res.*, 2022, **50**, 5467–5481.

61 (*a*) F. A. Taiwo, Mechanism of tiron as scavenger of superoxide ions and free electrons, *Spectroscopy*, 2008, **22**, 491–498; (*b*) C. Slator, Z. Molphy, V. McKee, C. Long, T. Brown and A. Kellett, Di-copper metallodrugs promote NCI-60 chemotherapy *via* singlet oxygen and superoxide production with tandem TA/TA and AT/AT oligonucleotide discrimination, *Nucleic Acid Res.*, 2018, **46**, 2733–2750; (*c*) N. McStay, C. Slator, V. Singh, A. Gibney, F. Westerlund and A. Kelllett, Click and cut: a click chemistry approach to developing oxidative DNA damaging agents, *Nucleic Acid Res.*, 2021, **49**, 10289–10308.

62 S. Goldstein, G. Merenyi, A. Russo and A. Samuni, The role of oxoammonium cation in the SOD-mimic activity of cyclic nitroxides, *J. Am. Chem. Soc.*, 2003, **125**, 789–795.

63 N. McStay, C. Slator, V. Singh, A. Gibney, F. Westerlund and A. Kellett, Click and Cut: a click chemistry approach to developing oxidative DNA damaging agents, *Nucleic Acid Res.*, 2021, **49**, 10289–10308.

64 C. Slator, Z. Molphy, V. McKee, C. Long, T. Brown and A. Kellett, Di-copper metallodrugs promote NCI-60 chemotherapy *via* singlet oxygen and superoxide

production with tandem TA/TA and AT/AT oligonucleotide discrimination, *Nucleic Acid Res.*, 2018, **46**, 2733–2750.

65 H. Leonhardt, H. P. Rhan, P. Weinzierl, A. Sporbert, T. Cremer, D. Zink and M. C. Cardoso, Dynamics of DNA replication factories in living cells, *J. Cell Biol.*, 2000, **149**, 271–280.

66 R. M. Bringhurst and P. A. Schaffer, Cellular stress rather than stage of the cell cycle enhances the replication and plating efficiencies of herpes simplex virus type 1 ICP0-viruses, *J. Virol.*, 2006, **80**, 4528–4537.

67 TUNEL Assay (commercial) Kit detects the DNA fragmentation of apoptotic cells by exploiting the fact that the DNA breaks expose many 3′-hydroxyl ends. These hydroxyl groups can then serve as starting points for terminal deoxynucleotidyl transferase (TdT), which adds deoxyribonucleotides in a template-independent fashion. Addition of the deoxythymidine analog 5-bromo-2′-deoxyuridine 5′-triphosphate (BrdUTP) to the TdT reaction serves to label the break sites. Once incorporated into the DNA, BrdU can be detected by an anti-BrdU antibody using standard immunohistochemical technique.